Spectroscopic and Photochemical Properties of Open-Chain Carotenoids

Harry A. Frank,*,† Jesusa S. Josue,† James A. Bautista,† Ineke van der Hoef,‡ Frans Jos Jansen,‡ Johan Lugtenburg,‡ Gary Wiederrecht,§ and Ronald L. Christensen||

Department of Chemistry, 55 North Eagleville Road, University of Connecticut, Storrs, Connecticut 06269-3060, Gorlaeus Laboratories, Leiden University, 2300 RA Leiden, The Netherlands, Chemistry Division, Argonne National Laboratories, Argonne, Illinois 60439, and Department of Chemistry, Bowdoin College, Brunswick, Maine 04011-8466

Received: August 27, 2001; In Final Form: November 28, 2001

The spectroscopic properties of open-chain, *all-trans*-C_{30} carotenoids having seven, eight and nine π-electron conjugated carbon−carbon double bonds were studied using steady-state absorption, fluorescence, fluorescence excitation and time-resolved absorption spectroscopy. These diapocarotenes were purified by high performance liquid chromatography (HPLC) prior to the spectroscopic experiments. The fluorescence data show a systematic crossover from dominant $S_1 \rightarrow S_0$ ($2^1A_g \rightarrow 1^1A_g$) emission to dominant $S_2 \rightarrow S_0$ ($1^1B_u \rightarrow 1^1A_g$) with increasing extent of conjugation. The low temperatures facilitated the determination of the spectral origins of the $S_1 \rightarrow S_0$ ($2^1A_g \rightarrow 1^1A_g$) emissions, which were assigned by Gaussian deconvolution of the experimental line shapes. The lifetimes of the S_1 states of the molecules were measured by transient absorption spectroscopy and were found to decrease as the conjugated chain length increases. The energy gap law for radiationless transitions is used to correlate the S_1 energies with the dynamics. These molecules provide a systematic series for understanding the structural features that control the photochemical properties of open-chain, diapocarotenoids. The implications of these results on the roles of carotenoids in photosynthetic organisms are discussed.

Introduction

Carotenoids are naturally occurring polyenes that play a number of important roles in photosynthesis. These pigments protect the photosynthetic apparatus against irreversible photodestruction either by quenching chlorophyll triplet states, which prevents the chlorophyll-sensitized formation of singlet state oxygen (a major oxidizing agent of chlorophyll),[1−3] by scavenging singlet oxygen directly,[4,5] or by dissipating excess excitation energy beyond that which is required for photosynthesis.[6] Carotenoids also function as light harvesting pigments supplementing the light-capturing ability of chlorophyll by absorbing light in regions of the visible spectrum where chlorophyll is not an efficient absorber.[7−11] The molecules then transfer the energy to chlorophyll, and ultimately the excitation is trapped in the reaction center pigment−protein complex where it initiates a series of electron-transfer events.[12] Carotenoids also may act as stabilizers of protein structure and facilitators of the assembly of pigment−protein complexes,[13−15] as regulators of energy flow,[6,15−21] or as redox cofactors.[22−25]

The most well-known naturally occurring carotenoid, β-carotene, is a C_{40} hydrocarbon with terminal isoprenoid rings and eleven π-electron conjugated carbon−carbon double bonds. Other naturally occurring carotenoids often contain functional group substitutions along the polyene chain and on the isoprenoid terminal rings. Simple polyenes and carotenoids have been studied extensively by optical spectroscopic methods, which have established that two low-lying excited electronic states, denoted S_1 and S_2, account for many of their spectroscopic properties. The ground state, S_0, and the first excited state, S_1, of the molecules possess A_g symmetry in the idealized C_{2h} point group. Electronic transitions between these states, i.e., $S_0 \rightarrow S_1$ ($1^1A_g \rightarrow 2^1A_g$) absorption or $S_1 \rightarrow S_0$ ($2^1A_g \rightarrow 1^1A_g$) fluorescence, are forbidden by symmetry. This is in contrast to the strongly allowed electronic transitions to and from S_0 and a higher excited state, denoted S_2, which has B_u symmetry. Recent literature suggests that for longer polyenes and carotenoids, other electronic states, e.g., a B_u^- state, may occur between S_2 ($1^1B_u^+$) and S_1 ($2^1A_g^-$).[26−28] Absorption from the ground state to the $1^1B_u^-$ state is forbidden by parity considerations, making this state difficult to detect. In the present work S_2 is referred to as "the B_u state", and the $S_0 \rightarrow S_2$ ($1^1A_g \rightarrow 1^1B_u$) and $S_2 \rightarrow S_0$ ($1^1B_u \rightarrow 1^1A_g$) transitions are considered strongly allowed.

A goal of the present work, embraced also by other researchers,[26,27,29−35] is to accurately determine the energies of the S_1 states of carotenoids and to elucidate how these energies are affected by changes in conjugation length. Unlike model polyenes that display highly resolved absorption and emission spectra at low temperatures, carotenoids exhibit broadening of their spectra due to increased vibrational complexity or conformational disorder modulated by the presence of substituents, especially rings and carbonyl functional groups, along the π-electron conjugated system. These complications are particularly evident for carotenoids and xanthophylls found in higher plants and algae. Few open-chain carotenoids are found in these species owing to the presence of the crtY gene that codes for the enzyme, lycopene cyclase, that forms isoprenoid rings.[36] Zeaxanthin and violaxanthin both possess rings, although in the case of violaxanthin, the double bonds in both terminal rings are saturated by the presence of epoxide groups. As a conse-

* For correspondence and/or reprints. Fax: 860-486-6558. E-mail: harry.frank@uconn.edu.
† University of Connecticut.
‡ Leiden University.
§ Argonne National Laboratories.
|| Bowdoin College.

10.1021/jp013321l CCC: $22.00
Published on Web 01/31/2002

heptaene

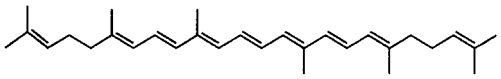

2,6,10,15,19,23-hexamethyl-2,6,8,10,12,14,16,18,22-tetracosanonaene

octaene

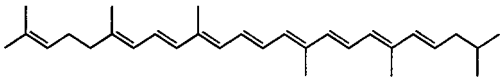

2,6,10,15,19,23-hexamethyl-2,6,8,10,12,14,16,18,20-tetracosanonaene

nonaene

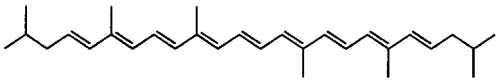

2,6,10,15,19,23-hexamethyl-4,6,8,10,12,14,16,18,20-tetracosanonaene

Figure 1. Structures of the C_{30} *all-trans* open-chain carotenoids.

quence the spectroscopic characteristics of violaxanthin are expected to be very similar to those of the open-chain carotenoids studied here.

In this work, a spectroscopic study of three open-chain, *all-trans*-C_{30} carotenoids is presented. These molecules are derived from spheroidene, the major carotenoid from the photosynthetic bacterium, *Rhodobacter (Rb.) sphaeroides* wild type, but lack the methoxy-functional group and the nonconjugated, floppy, C_{10}-terminal alkyl group of the parent molecule. The rationale for studying these derivatives is that without the substituents, higher resolved optical spectra may be observed that would facilitate the assignment of the positions of the excited-state energy levels. The structures of the C_{30} carotenoids, 2,6,10,-15,19,23-hexamethyl-2,6,8,10,12,14,16,18,22-tetracosanonaene, 2,6,10,15,19,23-hexamethyl-2,6,8,10,12,14,16,18,20-tetracosanonaene, and 2,6,10,15,19,23-hexamethyl-4,6,8,10,12,14,16,-18,20-tetracosanonaene are shown in Figure 1 and are hereafter are referred to as heptaene, octaene, and nonaene to indicate the number of double bonds in conjugation. The samples were purified by high performance liquid chromatography (HPLC) and studied using steady-state absorption, fluorescence, fluorescence excitation and time-resolved absorption spectroscopy. The open-chain analogues exhibit characteristics that are important for understanding the photochemical properties of carotenoids and polyenes in general, and for elucidating the specific molecular features that control the ability of their more highly conjugated counterparts to function in photosynthesis.

Materials and Methods

Synthesis. A description of the synthesis of the heptaene and nonaene molecules has already been published.[37] To prepare the C_{30} diapocarotene with eight conjugated double bonds, isovaleraldehyde (3-methylbutanal, Aldrich) was coupled to a C_5-phosphonate ester[38] in a Horner−Wadsworth−Emmons (HWE) reaction. The resulting ester was reduced to the corresponding C_{10} alcohol with Dibal-H. The C_{10} alcohol then was converted into a phosphonium salt by reacting with triphenylphosphonium hydrobromide, and coupled in a Wittig reaction to a C_{20} aldehyde that was prepared as follows: Geraniol (Aldrich) was oxidized with MnO_2 to yield geranial, which was coupled in a HWE reaction to a C_5-phosphonate nitrile.[39] The resulting nitrile was reduced with Dibal-H to the corresponding C_{15} aldehyde. This aldehyde was coupled in a HWE reaction to another C_5-phosphonate nitrile[40−42] to yield, after Dibal reduction, the C_{20} aldehyde.

Sample Preparation. The carotenoids were purified using a Millipore Waters 600E HPLC employing a 5 μm YMC C_{30} carotenoid column (4.6 mm × 250 mm). The mobile phase was 11:89 v/v methyl *tert*-butyl ether (MTBE)/methanol for the heptaene and the octaene and 38:62 v/v MTBE/methanol for the nonaene. The runs were isocratic at 1.0 mL/min. The heptaene, octaene and nonaene absorption bands were monitored at 400, 419 and 436 nm, respectively, using a photodiode array as a detector. The *all-trans* isomers were collected and dried with a gentle stream of nitrogen. The samples were kept in the dark until ready for use. EPA (ether/isopentane/ethanol, 5/5/2, v/v/v) was added to the samples prior to taking the absorption and fluorescence spectra at 293 and 77 K.

Spectroscopic Methods. *Steady-State Absorption and Fluorescence.* Absorption spectra of the samples in *n*-hexane and EPA solutions at 293 K and in EPA glasses at 77 K were recorded on a Cary 50 UV spectrometer. Absorption spectra were obtained from the samples in 4 mm (interior width) Suprasil square quartz cuvettes suspended in a cylindrical custom-made (Kontes) liquid nitrogen cryostat that was either empty for the experiment at 293 K or filled with liquid nitrogen for the experiment at 77 K. A gentle stream of He gas bubbled near the cuvette minimized agitation of the liquid nitrogen.

Fluorescence spectra were obtained using the same cuvette and cryostat used in absorption experiments. The fluorescence experiments were carried out using an SLM Instruments, Inc. Model 8000C spectrofluorometer, and the emission was detected by a Hamamatsu R928 photomultiplier (PMT) tube. An SLM Instrument Model WCTS-1 thermostatically cooled housing was used to reduce the PMT dark current. For fluorescence excitation spectroscopy the spectral profile of the incident light was monitored using HITC perchlorate as a quantum counter. A 450 W ozone free OSRAM XBO xenon arc lamp was used to excite the heptaene and octaene. The 463 or 477 nm lines from a Spectra-Physics argon ion laser Model 164 operating at a power of ∼50 mW was used for the nonaene.

For the heptaene, a 435 nm long-pass cutoff filter was placed between the sample and the emission monochromator for the 293 K experiment. A 455 nm filter was used for the 77 K experiment. The filters were positioned 90° to the excitation beam. The heptaene was excited at 421 nm for the experiment carried out at 293 K and at 431 nm for the 77 K experiment using 16 nm band-passes for both the excitation and emission monochromators. The SLM Aminco 8100 version 4.0 software automatically selects either signal averaging or integration whichever gives a better signal-to-noise ratio over the scanned wavelength range. The emission spectrum was then scanned at a relatively low amplifier gain and PMT voltage to obtain the maximum signal intensity that would occur in that spectral range. The wavelength at which the maximum signal was observed was used by the software to set the PMT voltage and amplifier gain to achieve a signal that registered 80% of the saturation maximum of the PMT. The spectrum was then scanned using these instrumental parameters. A spectral scan of the solvent blank was taken under identical conditions and subtracted from the spectral trace of the sample to remove contributions from fluorescence and Raman scattering by the solvent. A correction factor generated by a Spectral Irradiance 45W quartz-halogen tungsten coiled filament lamp standard was used to correct the fluorescence spectra.

The octaene was excited at 445 nm using the xenon arc lamp for the 293 K experiment and at 454 nm for the 77 K experiment

with 16 nm band-pass for both excitation and emission monochromators. A 470 nm long-pass cutoff filter was used for 293 K experiment, and a 460 nm cutoff filter was used for the 77 K experiment.

The nonaene was excited using an argon ion laser at 463 nm for the 293 K experiment and at 477 nm for the 77 K experiment. A 495 nm long-pass cutoff filter was used for both temperatures. The band-pass of the emission monochromator was 16 nm. To obtain a better signal-to-noise ratio for the very weak S_1 emission, the fluorescence spectrometer acquisition mode was set to photon counting and the emission was scanned from 600 to 900 nm for the sample at both temperatures. Starting the scan at 600 nm avoided rendering the spectrum off-scale owing to the presence of the relatively intense S_2 emission signal. The determination of instrument parameters, the removal of contributions from Raman scattering by the solvent, and the correction of the fluorescence spectra were carried out as described above.

Quantum Yield Measurements. The fluorescence quantum yields of the molecules were measured using Rhodamine 590 in methanol ($\phi_F = 0.95$)[43] as a standard. The evaluation of the quantum yields was based on the following equation:[44]

$$\phi_c = \phi_r\left(\frac{1-10^{-A_{r\lambda}}}{1-10^{-A_{c\lambda}}}\right)\left(\frac{I_{r\lambda}}{I_{c\lambda}}\right)\left(\frac{n_c^2}{n_r^2}\right)\left(\frac{D_c}{D_r}\right) \quad (1)$$

where ϕ_c and ϕ_r are the quantum yields of the carotenoid and reference solutions, respectively. $I_{c\lambda}$ and $I_{r\lambda}$ are the relative intensities of the excitation light at the wavelength, λ, for the carotenoid and standard solutions. $A_{c\lambda}$ and $A_{r\lambda}$ are the optical densities of the carotenoid and standard solutions at the wavelength, λ. n_c is the refractive index of the solvent for the carotenoid, and n_r is the refractive index of the solvent for the Rhodamine 590 standard. In these quantum yield experiments, the solvent for the carotenoid and standard solutions was the same (EPA), so the ratio of the indexes of refraction was unity. The ratio of the excitation light intensities was obtained using a reference photomultiplier. D_c and D_r are the integrated areas of the corrected emission spectra of the carotenoid and standard solutions obtained under identical instrumental conditions of slit width, gain, etc., and were derived from Gaussian fits to the emission line shapes (see below). To obtain comparable fluorescence areas for the weakly fluorescent sample and strongly fluorescent reference under these conditions, the concentration of the Rhodamine standard had to be approximately 5 orders of magnitude less than the carotenoid sample. To accomplish this, a linear calibration plot of integrated area of Rhodamine fluorescence versus optical density was made in the region from 1.00 to 0.001 absorbance where the optical density could be measured directly by absorption spectroscopy. The value of the Rhodamine optical density used in eq 1 was derived from a linear extrapolation of the calibration plot to the point corresponding to the measured integrated fluorescence area of the very dilute Rhodamine standard.

Transient Dynamics. Transient absorption data from the molecules in *n*-hexane were obtained at room temperature with a regeneratively amplified Ti:sapphire laser as described previously.[45,46] The system furnishes 140 fs transform limited pump pulses that are tunable from 470 to 820 nm. Typically 0.3−1 μJ was used to excite the molecules, and the spectral profiles were probed using a white light continuum generated by appropriate beam splitters passing part of the pump beam through a sapphire window. All of the samples were adjusted to an $S_0 \rightarrow S_2$ absorbance of 0.2 (1 cm cuvette) at the pump wavelength of 415 nm.

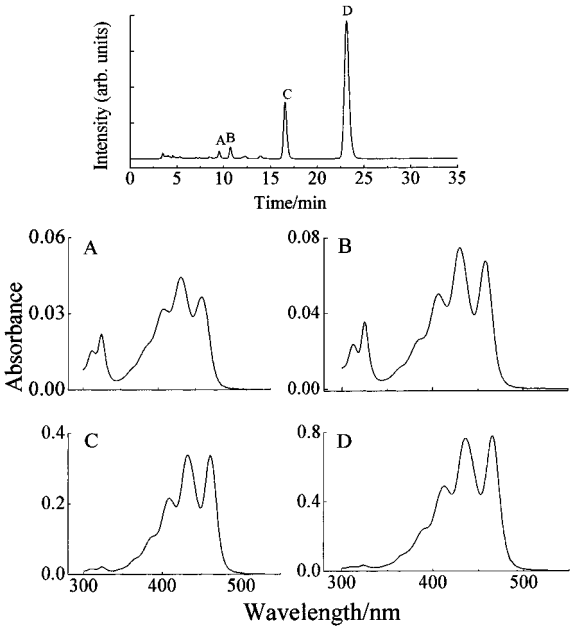

Figure 2. HPLC chromatogram of the nonaene molecule taken using a Millipore Waters 600E HPLC employing a 5 μm YMC C_{30} carotenoid column (4.6 mm × 250 mm). The mobile phase was 38:62 v/v MTBE/methanol, and the run was isocratic at 1.0 mL/min. The chromatogram monitored absorption at 436 nm using a photodiode array detector, which also yielded the spectra of the peaks labeled A−D.

Gaussian Deconvolution of Spectra. The instrument-corrected fluorescence spectra were transformed from a fixed band-pass wavelength scale to a fixed band-pass wavenumber scale by multiplying the fluorescence intensity by the square of the detection wavelength at each wavelength.[47] Gaussian deconvolutions of the line shapes were performed using Origin version 6.1 software. Starting values of the vibronic bands in wavenumbers were taken from estimates of the peaks and shoulders in the experimental spectra. The position, area, width, spacing and baseline of all the Gaussian components were allowed to vary unconstrained using a maximum of 50 iterations of the Levenberg−Marquardt algorithm. The number of Gaussian functions needed to fit the line shape also was systematically varied between 5 and 10, and the mean and standard deviation of each of the Gaussian components was determined.

Results

HPLC Analysis and Purification of the *All-Trans* Isomers. Figure 2 shows the HPLC chromatogram of the nonaene. The retention times of the different chain length carotenoids were very similar, with the most intense peak eluting after 20 min. The absorption spectra corresponding to the major chromatographic peaks have distinct, strongly allowed ($S_0 \rightarrow S_2$) transitions with extensive vibronic structure in the 350−500 nm region. For the nonaene (Figure 2) the longest wavelength vibrational feature in the spectrum (0−0) appeared at approximately 460 nm. The absorption spectra corresponding to the other peaks in the HPLC chromatogram show varying intensities of another absorption band at approximately 320 nm. This is the so-called "cis peak", which is usually found ~140 nm to shorter wavelength of the lowest energy spectral feature in the absorption spectrum and indicates different geometric isomers of the same carotenoid.[48,49] The intensity of this band is sensitive to the position of the cis double bonds, and the all-trans isomer is distinguished by a small cis peak. In each case, the all-trans carotenoid dominated the isomeric mixture. The

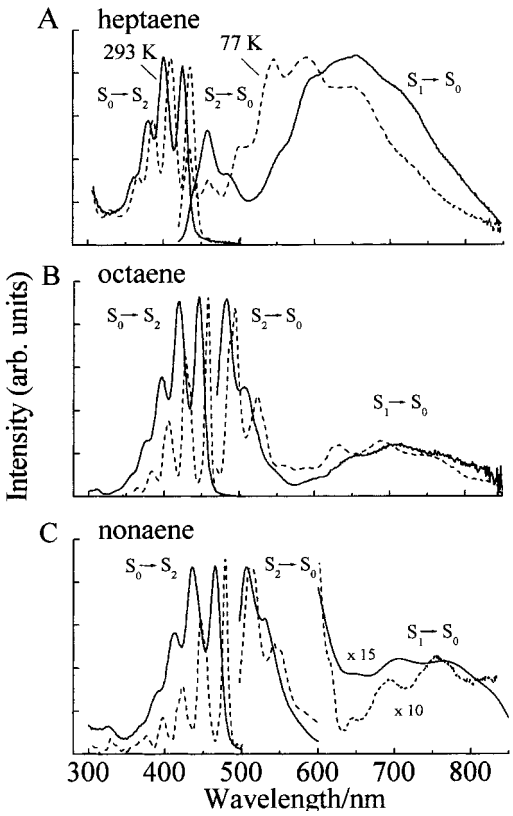

Figure 3. Overlay of absorption and fluorescence at 293 K (solid line) and 77 K (dashed line) from the molecules dissolved in EPA. The heptaene (A) was excited at 421 nm for the experiment carried out at 293 K and at 431 nm for the 77 K experiment. The octaene (B) was excited at 445 nm for the 293 K experiment and at 454 nm for the 77 K experiment. The nonaene (C) was excited using ~50 mW of power from an argon ion laser at 463 nm for the 293 K experiment and at 477 nm for the 77 K experiment.

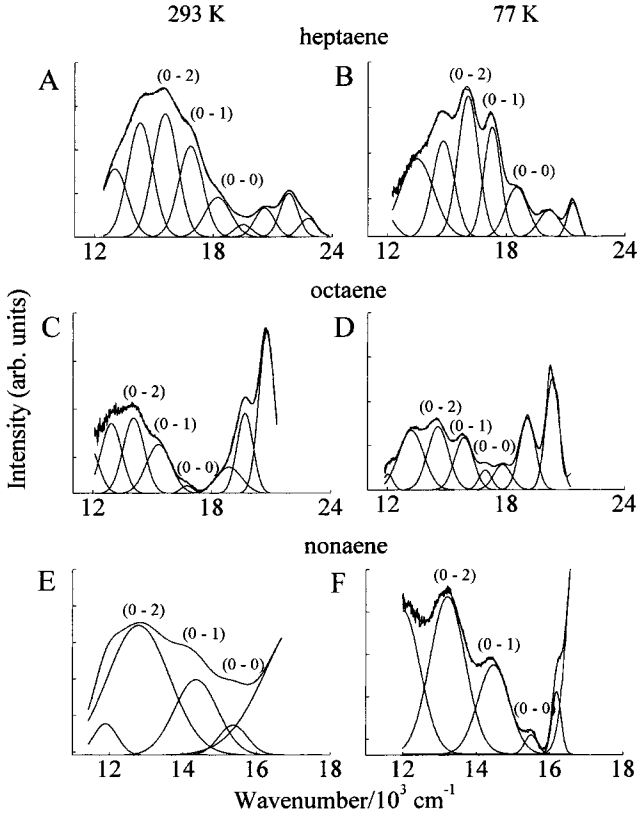

Figure 4. Instrument-corrected fluorescence spectra presented in Figure 3 replotted on a wavenumber scale and corrected for the variable band-pass as described in the Materials and Methods. The spectra were fit via Gaussian deconvolution of the line shapes using Origin version 6.1 software. The parameters describing the best fits to the emission spectra are given in Tables 1 and 2 for the molecular spectra taken at 293 (A, C, and E) and 77 K (B, D, and F), respectively.

HPLC protocol also removed impurities eluting at short (~3−8 min) retention times. These molecules absorb at <400 nm and are most likely less conjugated degradation products of the carotenoids. It was essential that these polyene impurities be removed because they have relatively high fluorescence yields and can adversely affect the fluorescence and the fluorescence excitation spectra.

Absorption and Fluorescence Spectra. The absorption spectra of the molecules in EPA at 77 and 293 K are shown in Figure 3 and are observed to red-shift with increasing extent of the π-conjugation. The full width at half-height of the 0−0 vibronic bands at 293 K ranged between ~750 and 840 cm^{-1}. The relative intensities of the vibronic bands of the carotenoids changed noticeably with the extent of π-electron conjugation and with temperature. Figure 3 shows that at 293 K, the most intense band in the absorption spectra for the heptaene molecule corresponds to the second vibronic feature, whereas for the octaene and nonaene molecules, the first and second vibronic features have roughly equal intensities. Lowering the temperature to 77 K resulted in a pronounced red shift of the spectra and a considerable narrowing of the 0−0 vibronic features to between ~360 and 710 cm^{-1}. The narrowing was particularly noticeable for the octaene and nonaene, which also showed substantial redistributions in the vibronic band intensities.

The fluorescence spectra shown in Figure 3 have two components. The first component is for the most part a mirror image of the $S_0 \rightarrow S_2$ absorption. The small Stokes shift between the origins of emission and absorption indicates that this part of the emission corresponds to the $S_2 \rightarrow S_0$ ($1^1B_u \rightarrow 1^1A_g$) transition. The second part of the emission has a maximum appearing at longer wavelengths and can be assigned to the $S_1 \rightarrow S_0$ ($2^1A_g \rightarrow 1^1A_g$) transition. The line shapes associated with this part of the spectra are broader than the $S_2 \rightarrow S_0$ emissions. However, upon lowering the temperature to 77 K, there is a significant enhancement in the resolution of the vibronic features of the emission spectra and also a blue shift of the $S_1 \rightarrow S_0$ emission maximum, most evident for the heptaene. This improved vibronic resolution has facilitated the analysis of the line shapes by Gaussian deconvolution (see Figure 4 and below). The final parameters for the fits are given in Tables 1 and 2. The fluorescence excitation spectra of the molecules were also obtained (data not shown), except in the case of the S_1 emission from the nonaene, which was precluded because a monochromatic laser was used for excitation. The excitation spectra were found to be in very good agreement with the absorption spectra.

Transient Absorption Experiments. Excitation of the all-trans isomers of the molecules in *n*-hexane at room temperature with a ~140 fs laser pulse at 415 nm resulted in a rapid buildup of $S_1 \rightarrow S_n$ absorption. The transient absorption bands were probed at 471 nm for the heptaene, 492 nm for the octaene, and 512 nm for the nonaene. The signals subsequently decayed with single-exponential kinetics as shown in Figure 5. The S_1 lifetimes determined from these data are 290 ± 30 ps for heptaene, 68 ± 7 ps for octaene, and 18 ± 2 ps for nonaene. The $S_1 \rightarrow S_n$ spectra both red-shift and narrow with increasing extent of π-electron conjugation.

Quantum Yields. The quantum yields of the $S_1 \rightarrow S_0$ and $S_2 \rightarrow S_0$ emissions are given in Table 3. The values decrease

TABLE 1: Fitting Parameters for the Gaussian Deconvolutions of the $S_1 \rightarrow S_0$ Emission Spectra of Heptaene, Octaene, and Nonaene in EPA at 293 K[a]

	vibronic band	$S_1 \rightarrow S_0$ 0 → 0	0 → 1	0 → 2	0 → 3	$S_0 \rightarrow S_2$ 0 → 0
heptaene	energy	18 120 ± 290	16 940 ± 70	15 650 ± 110	14 260 ± 95	23 530 ± 110
	λ	552	590	639	701	425
	Δ	1670 ± 440	1400 ± 290	1630 ± 160	1650 ± 95	840 ± 40
	A	0.04	0.20	0.37	0.27	
octaene	energy	16 740 ± 30	15 390 ± 50	14 100 ± 60	12 960 ± 30	22 420 ± 100
	λ	597	650	709	772	446
	Δ	930 ± 280	1370 ± 140	1310 ± 110	965 ± 300	750 ± 40
	A	0.09	0.22	0.25	0.24	
nonaene	energy	15 420 ± 90	14 220 ± 110	12 770 ± 35	11 920 ± 30	21 510 ± 95
	λ	649	703	783	839	465
	Δ	985 ± 310	1440 ± 140	1660 ± 260	760 ± 45	770 ± 40
	A	0.08	0.30	0.54	0.08	

[a] The energies and widths (Δ) are in cm^{-1} and the wavelengths (λ) are in nm units. The areas (A) of the vibronic peaks are relative within a spectrum and sum to unity. The uncertainties represent standard deviations derived from multiple fits to the experimental spectra. The spectral origins of the $S_0 \rightarrow S_2$ transitions and the line widths (cm^{-1}) based on the absorption spectra are also given.

TABLE 2: Fitting Parameters for the Gaussian Deconvolutions of the $S_1 \rightarrow S_0$ Emission Spectra of Heptaene, Octaene, and Nonaene in EPA at 77 K[a]

	vibronic band	$S_1 \rightarrow S_0$ 0 → 0	0 → 1	0 → 2	0 → 3	0 → 4	0 → 5	$S_0 \rightarrow S_2$ 0 → 0
heptaene	energy	18 540 ± 40	17 270 ± 15	16 010 ± 50	14 750 ± 50	13 490 ± 40	11 860 ± 510	22 990 ± 110
	λ	539	579	625	678	741	843	435
	Δ	1260 ± 160	1100 ± 120	1220 ± 30	1280 ± 55	1600 ± 340	1630 ± 520	710 ± 40
	A	0.10	0.20	0.27	0.22	0.19	0.04	
octaene	energy	16 970 ± 40	15 850 ± 35	14 530 ± 40	13 210 ± 30	12 070 ± 45		21 840 ± 100
	λ	589	631	688	757	829		458
	Δ	825 ± 200	1100 ± 80	1240 ± 60	1350± 170	740 ± 370		390 ± 20
	A	0.07	0.23	0.34	0.33	0.04		
nonaene	energy	15 500 ± 80	14 460 ± 25	13 260 ± 20	11 925 ± 40			20 920 ± 90
	λ	645	692	754	839			478
	Δ	640 ± 320	1250 ± 130	1000 ± 65	1700 ± 350			360 ± 20
	A	0.06	0.23	0.33	0.36			

[a] The energies and widths (Δ) are in cm^{-1} and the wavelengths (λ) are in nm units. The areas (A) of the vibronic peaks are relative within a spectrum and sum to unity. The uncertainties represent standard deviations derived from multiple fits to the experimental spectra. The spectral origins of the $S_0 \rightarrow S_2$ transitions and the line widths (cm^{-1}) based on the absorption spectra are also given.

with increasing extent of π-electron conjugation. The quantum yields can be used with the lifetimes of the S_1 states to calculate the radiative rate constants associated with the $S_1 \rightarrow S_0$ deactivation. The relevant equations are

$$\phi_{S_1 \rightarrow S_0} = \frac{k_r}{k_r + k_{nr}} = k_r \tau_{S_1 \rightarrow S_0} \quad (2)$$

$$k_r = \frac{\phi_{S_1 \rightarrow S_0}}{\tau_{S_1 \rightarrow S_0}} \quad (3)$$

where k_r is the radiative rate constant, k_{nr} is the nonradiative rate constant, τ is the lifetime of the S_1 state and ϕ is the quantum yield of the $S_1 \rightarrow S_0$ fluorescence emission. The values for the radiative rate constants computed in this manner are given in Table 3.

Discussion

The crossover from the $S_1(2^1A_g) \rightarrow S_0(1^1A_g)$ emission in the heptaene to the dominant, $S_2(1^1B_u) \rightarrow S_0(1^1A_g)$ fluorescence of the nonaene parallels similar changes from $S_1 \rightarrow S_0$ to $S_2 \rightarrow S_0$ emissions in simple polyenes,[16] apocarotenols,[50] spheroidenes,[51] analogues of β-carotene,[29,52] and apocarotenes.[37] Although fluorescence quantum yields are sensitive to structural details, the relatively abrupt change to $S_2 \rightarrow S_0$ emissions invariably occurs for molecules with seven or eight conjugated bonds. At first glance, the crossover might be attributed to the decrease in the rate of $S_2 \rightarrow S_1$ internal conversion following the "energy-gap law".[53] Large S_2-S_1 energy gaps may result in $S_2 \rightarrow S_1$ internal conversion rates that become sufficiently small to allow the relatively strong $S_2 \rightarrow S_0$ fluorescence to compete with radiationless decay processes, leading to violations of Kasha's Rule.[54] This model accounts for $S_2 \rightarrow S_0$ emissions in several aromatic molecules, all of which are characterized by large S_2-S_1 energy differences.[53] And the S_2-S_1 energy difference at which $S_2 \rightarrow S_0$ fluorescence is observed in polyenes and carotenoids ($\sim$5000 cm^{-1}) is consistent with the thresholds for S_2 emissions in a variety of aromatic systems.

However, the rather abrupt changeover from $S_1 \rightarrow S_0$ to $S_2 \rightarrow S_0$ emissions is not easily reconciled with the very modest increase in S_2-S_1 energy differences in previously studied polyenes and carotenoids.[16,29,50-52,55] Indeed, the three molecules studied here have similar S_2-S_1 energy gaps (5200, 5700, and 6100 cm^{-1} at 293 K). Given this small variation in S_2-S_1 energy gap, the rate of $S_2 \rightarrow S_1$ radiationless decay should be relatively insensitive to conjugation length. In fact, the expected increase in the density of vibrational "accepting" modes in longer polyenes (generally thought to be C−C stretches[56]) should contribute to *increases* in $S_2 \rightarrow S_1$ internal conversion rates with increasing conjugation length, counteracting any *decreases* due to widening of the S_2-S_1 energy gap. Recent investigations of $S_2 \rightarrow S_0$ fluorescence quantum yields in carotenes[29,52] and spheroidenes[55] indicate $S_2 \rightarrow S_1$ internal conversion rates that

TABLE 3: Electronic Energies of the S_1 and S_2 States, Quantum Yields, ϕ_f, of $S_2 \rightarrow S_0$ and $S_1 \rightarrow S_0$ Emission, S_1 Lifetimes, τ_{S_1}, and Radiative Rate Constants, k_r, of the Carotenoids

molecule	no. of conj −C=C− bonds	solvent	T/K	spectral origins (cm^{-1}) of transitions $S_1 \rightarrow S_0$	spectral origins (cm^{-1}) of transitions $S_0 \rightarrow S_2$	$10^5\phi_f$ $S_1 \rightarrow S_0$	$10^5\phi_f$ $S_2 \rightarrow S_0$	τ_{S_1}/ps	$10^{-5}k_r$ $(S_1 \rightarrow S_0)$/ s^{-1}	ref
heptaene	7	*n*-hexane	293	18 160 ± 40[a]	23 500			290 ± 30		
		EPA	293	18 120 ± 290[a]	23 500	12 ± 6	2.2 ± 1.1		4.1 ± 2.1	
		EPA	77	18 540 ± 40[a]	23 000					
3,4,7,8-tetrahydrospheroidene	7	*n*-hexane	RT	18 400[a]	23 200 ± 500		12.6 ± 1.9	407 ± 23		51
octaene	8	*n*-hexane	293	16 840 ± 170[a]	22 500			68 ± 7		
		EPA	293	16 740 ± 30[a]	22 400	2.3 ± 1.6	2.7 ± 1.8		3.4 ± 2.4	
		EPA	77	16 970 ± 40[a]	21 800					
3,4,5,6-tetrahydrospheroidene	8	*n*-hexane	RT	16 700[a]	22 300 ± 500		22 ± 5	85 ± 5		51
nonaene	9	*n*-hexane	293	15 120 ± 220[a]	21 500			18 ± 2		
		EPA	293	15 420 ± 90[a]	21 500	0.14 ± 0.1	1.7 ± 1.2		0.8 ± 0.6	
		EPA	77	15 500 ± 80[a]	20 900					
3,4-dihydrospheroidene	9	*n*-hexane	RT	15 300[a]	21 300 ± 500		27 ± 3	25.4 ± 0.9		51
violaxanthin	9	*n*-hexane	293	14 880 ± 90[a]	21 200			23.9		71
		methanol	RT	14 470 ± 90[c]						31
neurosporene	9	*n*-hexane	170	15 300[a]						34
		n-hexane	295	15 300[a]	21 300			21		34
spheroidene	10	*n*-hexane	200	14 200[a]						34
		n-hexane	295	14 200[a]						34
		n-hexane	RT	14 200 ± 50[a]	20 600 ± 400		12.0 ± 2.5	8.7 ± 0.1		51
		n-hexane	293	13 400 ± 90[c]						32
		n-hexane	186	13 400 ± 90[c]						32
		crystalline	RT	14 200[b]						26
lycopene	11	*n*-hexane	170	13 300 ± 300[a]						35
		n-hexane	295	13 300 ± 300[a]	19 900			4.7		35
		crystalline	RT	13 200[b]						27

[a] Fluorescence, [b]Resonance Raman, [c]$S_1 \rightarrow S_2$ absorption.

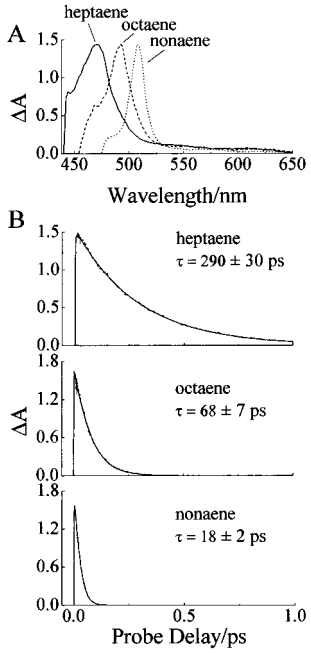

Figure 5. Decay dynamics and transient absorption spectra from the heptaene, octaene, and nonaene dissolved in *n*-hexane and taken at 293 K. The transient absorption bands were probed at 471 nm for the heptaene, 492 nm for the octaene, and 512 nm for the nonaene. The signals decayed with single-exponential kinetics to zero yielding S_1 lifetimes of 290 ± 30 ps for heptaene, 68 ± 7 ps for octaene, and 18 ± 2 ps for nonaene.

are remarkably insensitive to conjugation length. For example, Andersson et al.[29] estimate an approximately 2-fold *decrease* in the rate of $S_2 \rightarrow S_1$ internal conversion in going from $N = 5$ to $N = 13$ in a series of β-carotene analogues. Frank et al.[55] observed comparable changes (though in the opposite direction) in k_{ic} in a series of spheroidene analogues with $N = 7-13$. The heptaene, octaene and nonaene molecules studied here display only a very small (less than a factor of 2) variation in the $S_2 \rightarrow S_0$ fluorescence quantum yields (Table 3). The basic conclusion is that the $S_2 \rightarrow S_1$ internal conversion rates are essentially independent of conjugation length for these carotenoids.

There is both theoretical[57] and spectroscopic[26,27,33] evidence for a low-lying $^1B_u^-$ state in longer carotenoids ($N = 9-13$), intermediate in energy between the $2^1A_g^-$ state (designated as S_1 in this paper) and the $1^1B_u^+$ state (S_2 in this paper). Koyama et al.[27] further have postulated that the $^1B_u^-$ state may modulate and/or dominate the dynamics of $1^1B_u^+$ relaxation. However, the $1^1B_u^-$ state must lie above the $1^1B_u^+$ state in the more extensively studied, well-understood shorter polyenes ($N = 4-8$), which show extremely efficient $1B_u^+ \rightarrow 2A_g^-$ internal conversion. Furthermore, the relative insensitivity of $1B_u^+ \rightarrow 2A_g^-$ internal conversion rates to conjugation lengths is not consistent with the introduction of a rapid kinetic pathway for those polyenes and carotenoids for which $E(^1B_u^-) < E(^1B_u^+)$. Thus, current data on the dynamics of polyenes and carotenoids do not support an important role for a low-lying $^1B_u^-$ state in mediating internal conversion.

The "crossover" to $S_2 \rightarrow S_0$ fluorescence in longer polyenes and carotenoids is most easily explained by increases in the rates of $S_1 \rightarrow S_0$ nonradiative decay due to a combination of smaller S_1-S_0 energy gaps and the increased density of S_0 accepting modes in larger molecules. This leads to the disappearance of $S_1 \rightarrow S_0$ fluorescence, allowing the weak, residual $S_2 \rightarrow S_0$ fluorescence to dominate the emissions of longer conjugated systems. This picture is reinforced by the almost 20-fold decrease in $S_1 \rightarrow S_0$ lifetimes observed in going from the heptaene ($\tau = 290 \pm 30$ ps) to the nonaene ($\tau = 18 \pm 2$ ps). Given the dominance of nonradiative process in these systems, the S_1 lifetimes indicate a similar 20-fold increase in the $S_1 \rightarrow S_0$ nonradiative decay rates and should result in a parallel decrease in $S_1 \rightarrow S_0$ fluorescence quantum yields. This

is confirmed by the $S_1 \rightarrow S_0$ quantum yields given in Table 3. The $S_1 \rightarrow S_0$ quantum yields decrease by roughly 2 orders of magnitude with increasing conjugated chain length from seven to nine conjugated carbon−carbon double bonds. The $S_2 \rightarrow S_1$ internal conversion rates (and $S_2 \rightarrow S_0$ fluorescence yields) are relatively constant for these molecules, and the sharp decrease in $S_1 \rightarrow S_0$ fluorescence accounts for the increase in the ratio of $S_2 \rightarrow S_0/S_1 \rightarrow S_0$ emission.

The prominent vibronic bands for the $S_1 \rightarrow S_0$ transitions are given in Tables 1 and 2. The (0−0), (0−1), (0−2), etc., notation refers to unresolved progressions of the totally symmetric C−C and C=C stretching modes that dominate the Franck−Condon envelopes of polyene/carotenoid electronic spectra.[37,58] The vibronic spacings of ~1200 cm^{-1} thus should be viewed as "hybrids" of the C−C and C=C modes observed in higher resolution polyene spectra. The consistency of the vibronic intervals indicated in Tables 1 and 2 provides additional confidence in the validity of the Gaussian fits and of the electronic origins derived for the $S_1 \rightarrow S_0$ transitions. It is important to point out that the electronic origins ((0−0) bands) for the symmetry-forbidden $S_1 \rightarrow S_0$ transitions should be weak (or nonexistent) with the vibrational progressions built on nontotally symmetric (b_u) promoting modes due to Herzberg−Teller vibronic coupling.[59] For symmetric polyenes under conditions (e.g., in supersonic jets or in mixed-crystal environments) that retain their centers of inversion, $S_1 \leftrightarrow S_0$ (0−0)'s are missing with the electronic transitions being built on b_u false origins.[60] However, the most prominent b_u promoting modes are in-plane bending modes with very low frequency, <100 cm^{-1} in long polyenes. The distinction between (0−0) bands and b_u false origins thus will not be detectable in the relatively low-resolution spectra (vibronic bandwidths >500 cm^{-1}) presented here. Furthermore, solvent perturbations and asymmetric substitutions result in (0−0) intensities that are comparable to those of false origins.[60,61] The electronic origins of $S_1 \leftrightarrow S_0$ spectra in solution thus should be viewed as a complicated superposition of spectra of distorted and undistorted molecules, all of which contribute to the (0−0) line shapes in typical condensed phase spectra.

The present work plus previously published data on longer diapocarotenes provides a systematic view of the $S_0 \rightarrow S_2$ and $S_1 \rightarrow S_0$ transitions energies ((0−0) bands) in a common solvent (room temperature *n*-hexane) as a function of conjugation length ($N = 7-11$). These data are summarized in Figure 6. Linear least-squares fits of transition energies versus $1/N$ ($E = A + B/N$) also are indicated (Figure 6) and give $A = 14\,000 \pm 360$ cm^{-1} and $B = 66\,000 \pm 3000$ cm^{-1} for $S_0 \rightarrow S_2$ and $A = 4500 \pm 300$ cm^{-1} and $B = 96\,700 \pm 2600$ cm^{-1} for the $S_1 \rightarrow S_0$ transitions. These fits clearly will be useful in extrapolating transition energies to longer diapocarotenoids such as spirilloxanthin ($N = 13$). It also is interesting to compare the data for the $S_0 \rightarrow S_2$ transition with that obtained from a series of α,ω-di-*tert*-butyl polyenes in room temperature *n*-pentane ($A = 14\,350 \pm 150$ cm^{-1} and $B = 76\,000 \pm 1200$ cm^{-1}).[62] (See dashed line in Figure 6.) The systematic red shifts in the carotenoids can be explained by the preferential stabilization of the $\pi\pi^*$ excited states by the isoprene methyl groups, though the two sets of polyene $S_0 \rightarrow S_2$ transitions converge to almost identical limits as $N \rightarrow \infty$.

It also is useful to compare the electronic origins of the $S_1 \rightarrow S_0$ and $S_0 \rightarrow S_2$ transitions of the open-chain, diapocarotenes with those of comparable apocarotenes.[37] The presence of a terminal double bond within a β-ionylidene ring gives rise to steric repulsions between the methyl groups on the ring and the polyene chain. This forces the ring double bond out of the plane of conjugation of the other double bonds, resulting in a blue shift of the electronic transitions. A comparison of the molecules studied here with their apo counterparts[37] indicates shifts of 1540, 1210, and 670 cm^{-1} for the $S_0 \rightarrow S_2$ absorptions of the heptaene, octaene, and nonaene in 77 K EPA. The corresponding shifts for the $S_1 \rightarrow S_0$ (0−0)'s are smaller (880, 930, and 810 cm^{-1}) and relatively insensitive to the length of conjugation. These comparisons should be extended to longer carotenoids to develop a more systematic understanding of the difference between transition energies in the diapo, apo, and parent carotenoids. The nature of the terminal double bonds should be less significant with increasing conjugation. For example, the difference between the $S_0 \rightarrow S_2$ transition energies of lycopene ($N = 11$)[63] and its corresponding apocarotene, γ-carotene,[64] in room temperature *n*-hexane is about 400 cm^{-1}.

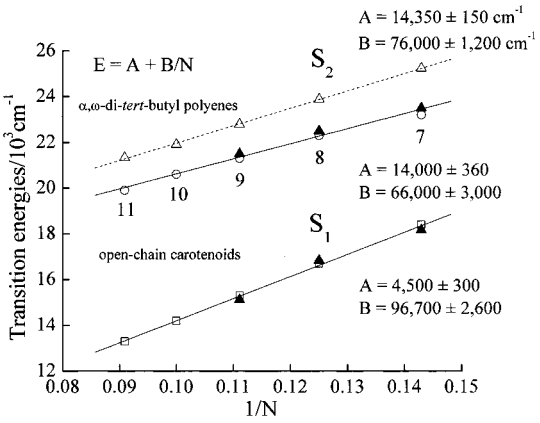

Figure 6. $S_0 \rightarrow S_2$ and $S_1 \rightarrow S_0$ transition energies of several open-chain carotenoids determined by absorption and fluorescence spectroscopy in room temperature *n*-hexane solutions as a function of the inverse ($1/N$) of conjugation length ($N = 7-11$). The number of conjugated carbon carbon double bonds is indicated for the molecules: 7, heptaene and 3,4,7,8-tetrahydrospheroidene; 8, octaene and 3,4,5,6-tetrahydrospheroidene; 9, nonaene, neurosporene, and 3,4-dihydrospheroidene; 10, spheroidene; and 11, lycopene. The heptaene, octaene, and nonaene molecules studied here are indicated by closed triangles. The other data points (open circles) are taken from published data summarized in Table 3. The uncertainties in the numbers determined here or reported in the literature are given in Table 3 and are either comparable to or smaller than the size of the symbols on the plot. Linear least-squares fits of transition energies versus $1/N$ ($E = A + B/N$) also are indicated. Data for the α,ω-di-*tert*-butyl polyenes (dashed line) are from Knoll and Schrock.[62]

It has been suggested[55,65,66] that the energy gap law for radiationless transitions[53] in the weak coupling limit accounts for the decrease in the S_1 lifetime of carotenoids and polyenes as a result of the narrowing of the energy difference between S_1 and S_0 following:

$$k_{ic}(S_1 \rightarrow S_0) = \frac{m_1}{(\Delta E m_3)^{1/2}} \exp\left[-\gamma \frac{\Delta E}{m_3}\right] \qquad (4)$$

where m_1, m_2, and m_3, are parameters defined as

$$m_1 = \frac{C^2(2\pi)^{1/2}}{\hbar} \qquad m_2 = d\Delta_M{}^2 \qquad m_3 = \hbar\omega_M$$

and in terms of these parameters

$$\gamma = \ln(2\Delta E/m_2 m_3) - 1 \qquad (5)$$

$k_{ic}(S_1 \rightarrow S_0)$ is the internal conversion rate constant for the radiationless deactivation of the S_1 state. For the molecules

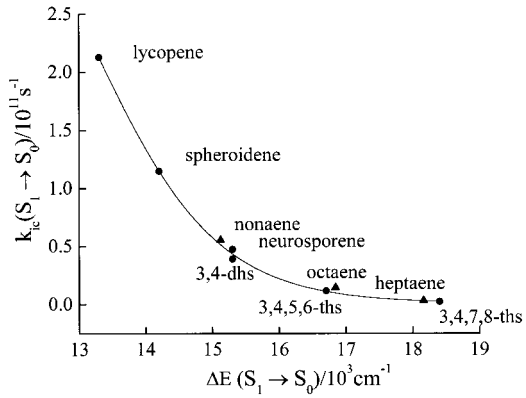

Figure 7. Rate constants for the decay of the S_1 states of open-chain carotenoids plotted against the values of the energies obtained from fluorescence spectroscopy. All data correspond to experiments done at room temperature in *n*-hexane solutions. The data are fit by the exponential function given in eq 4. The parameters were $m_1 = 5.34 \times 10^{14}$ cm^{-1} s^{-1}, which corresponds to $C = 31.0$ cm^{-1}, and $m_2 = 6.52$, and $m_3 = \hbar\omega_M$ was fixed at 1600 cm^{-1}. The uncertainties in the numbers determined here or reported in the literature are given in Table 3 and are either comparable to or smaller than the size of the symbols on the plot.

studied here, this is approximated by the reciprocal of the measured S_1 lifetime ($\tau_{S_1} = 1/(k_{ic} + k_r) \approx 1/k_{ic}$). ΔE is the $S_1 - S_0$ ($2^1A_g - 1^1A_g$) energy difference, C is a vibronic coupling matrix element, $\hbar\omega_M$ is the energy of the accepting vibrational mode, and γ can be related to the relative displacement, Δ_M, of the potential surfaces of the S_1 and S_0 electronic states. d is the number of degenerate accepting modes. The dynamics and the fluorescence spectra were measured at room temperature in *n*-hexane solutions, and the rate constants plotted against the values of S_1 energies obtained from the fluorescence spectra. The data points may be fit by the exponential function given in eq 4. Figure 7 shows the fit obtained when the three parameters m_1, m_2, and m_3, are optimized using the data presented in Table 3. The values for C derived from the parameter, m_1, were found to depend strongly on the value of the m_3 parameter. It has been shown[67] that the dominant accepting mode ($\hbar\omega_M$) for β-carotene has a vibrational frequency of ~1600 cm^{-1}. If $m_3 = \hbar\omega_M$ is restricted to a range of values between 1000 and 5000 cm^{-1}, consistent with this magnitude of vibrational accepting mode energies, C values derived from the parameter m_1 fell within the range 31.0−446 cm^{-1} and yielded plots virtually identical with that shown in Figure 7. The γ values derived from eq 5 using the $S_1 - S_0$ energies for ΔE, a fixed value of value of 1600 cm^{-1} for m_3, and the fit value of 6.52 for m_2, were 0.25 for heptaene, 0.17 for octaene and 0.08 for nonaene. These values of C and γ are consistent with a weak coupling limit for radiationless decay from the S_1 states of open-chain carotenoids. In this limit, $\Delta E \gg C$ (ΔE spans the range 13 300 to 18 400 cm^{-1}) and the γ values are well within the range of what is expected for π-electron conjugated systems having these $S_1 - S_0$ energy gaps.[53,66,68−70]

It is instructive to compare the S_1 energies and lifetimes of diapocarotenoids that only differ with respect to their nonconjugated end groups. The nonaene (18 ps/15 120 cm^{-1}), violaxanthin (24 ps/14 900 cm^{-1}),[71] neurosporene (21 ps/15 300 cm^{-1}), and 3,4-dihydrospheroidene (27 ps/15 300 cm^{-1} in methanol) all may be considered as "diapo" carotenes with $N = 9$. (See Table 3.) This establishes the primary importance of the number of double bonds in determining the energetics and dynamics of a given series of carotenoids (diapo, apo, or the parent carotenoid). The nature of the unconjugated end groups thus appears to have remarkably little influence either on the energetics or dynamics of the S_1 state. This also supports the notion that $S_1 \rightarrow S_0$ internal conversion in diapocarotenoids can be described by a common set of coupling and displacement parameters as described by the energy gap law (see above).

This study provides a systematic look at the effect of temperature on the $S_0 \rightarrow S_2$ and $S_1 \rightarrow S_0$ transitions in carotenoids (Figure 3). Most obvious is the increase in vibronic resolution at 77 K, which enhances the ability to accurately determine the energies of individual vibronic bands. The decrease in vibronic line widths presumably can be traced to the reduction of conformational disorder at lower temperatures. The $S_0 \rightarrow S_2$ and $S_2 \rightarrow S_0$ transitions also undergo significant red shifts (~400 cm^{-1}), which can be explained both by the reduction in conformational disorder (the conjugated polyene segments may become more planar at lower temperature) and by the increase in solvent polarizability due to the significant contraction in volume in forming the 77 EPA glass (V(77 K)/V(295 K) = 0.77). The $S_0 \leftrightarrow S_2$ transition energy in polyene hydrocarbons shows a linear dependence on solvent polarizability.[72]

Although the forbidden, $S_1 \rightarrow S_0$ transition in polyene hydrocarbons is considerably less sensitive to solvent polarizability,[72] the systematic *blue shift* of ~420, 230, and 80 cm^{-1} of this transition for the heptaene, octaene, and nonaene samples in going from room temperature to 77 K has not previously been noted in polyene spectroscopy. One explanation is that the high viscosity of the low-temperature glass and the short excited-state lifetimes prevent the S_1 state from relaxing to its most stable conformation, which is significantly different than the conformations of the S_0 and S_2 states. As seen in Figure 3, the $S_0 \rightarrow S_2$ transition shows significant enhancement of the intensity of the (0−0) band in the low temperature samples. Though most evident for the octaene and nonaene, this effect can be traced to a significantly smaller geometry change between the S_0 and S_2 states in the 77 K samples. The $S_1 \rightarrow S_0$ transitions, on the other hand, show long progressions in the C−C and C═C stretching modes, indicating substantial differences in the π bond orders in the S_0 and S_1 states. Although the blue shift of the $S_1 \rightarrow S_0$ transition, and corresponding reduction in the S_2-S_1 energy gap, appears to be less pronounced with increasing conjugation, the effects of temperature and solvent viscosity on carotenoid excited states merit further scrutiny. At a minimum, the results summarized in Figure 3 suggest the need for caution in extrapolating between the S_1 energies and dynamics of carotenoids in room-temperature organic solvents and carotenoids in rigid protein matrixes in photosynthetic systems.

The data presented here are helping elucidate the energy relationships between the excited states of carotenoids that act as light harvesting pigments in photosynthetic systems and chlorophylls that are acceptors of this energy. Because the open-chain carotenoids are most readily found in the pigment−protein complexes of photosynthetic bacteria, where bacteriochlorophyll (BChl) *a* is the primary pigment, it is interesting to compare the S_1 states of these molecules. The lowest S_1 state energies of BChl *a* in the LH1 and LH2 complexes from photosynthetic bacteria are ~11 200 cm^{-1} (BChl absorption at 890 nm, e.g., in the LH1 complex from *Rhodospirillum rubrum*), ~11 400 cm^{-1} (BChl absorption at 875 nm, e.g., in the LH1 complex from *Rb. sphaeroides*), and ~11 760 cm^{-1} (BChl absorption at 850 nm, e.g., in the LH2 complexes from *Rb. sphaeroides* and *Rhodopseudomonas acidophila*). The linear plot shown in Figure 6 extrapolated to $N = 13$ gives 11 975 cm^{-1} for the S_1 state

energy of spirilloxanthin, the longest naturally occurring diapocarotenoid. This is still higher than the lowest S_1 state energy for BChl *a* in a light harvesting complex. Thus, from an energetics standpoint, transfer from the S_1 state of any carotenoid to BChl is favorable. However, the exponential increase in the rate constant for radiationless decay of the S_1 states of carotenoids with decreasing energy gap (eq 4) between S_1 and S_0 may reduce the probability that S_1 is the sole energy donor state for the longer conjugated molecules. Transfer from the S_2 (1^1B_u) state to BChl has also been shown to be important in LH2 complexes.[73,74] It is interesting to note that the best fit line for the diapocarotenoids (Figure 6) predicts $\lambda(0-0) = 524$ nm for the $S_0 \rightarrow S_2$ transition of spirilloxanthin in *n*-pentane. This compares remarkably will with $\lambda(\text{exp}) = 526$ nm,[75] further supporting the validity of our fits.

Conclusions

These studies on C_{30} carotenoids provide a definitive set of data for the S_1 and S_2 state energies and S_1 state dynamics of open-chain carotenoids. Taken together with data previously published, the energies of the states were found to be well described by the simple linear relationship summarized in Figure 6. The dynamics of the S_1 states of the molecules and the trends in the fluorescence spectral profiles and yields are consistent with an exponential decrease in the nonradiative rate constant for decay from the S_1 state rationalized by the energy gap law for radiationless transitions given by eq 4. The data provide a firm foundation from which the optical spectroscopy and excited state dynamics of structurally more complex carotenoids and xanthophylls may be better understood.

Acknowledgment. This work has been supported in the laboratory of H.A.F. by grants from the National Institute of Health (GM-30353), the National Science Foundation (MCB-9816759), and the University of Connecticut Research Foundation, and to J.L. from The Netherlands Foundation of Chemical Research (SON), which is financed by The Netherlands Organization for the Advancement of Pure Research (NWO). The work at Argonne National Laboratory was supported by the Office of Basic Energy Sciences, Division of Chemical Sciences, U.S. Department of Energy under contract W-31-109-Eng-38. R.L.C. acknowledges the donors of the Petroleum Research Fund, administered by the American Chemical Society, for support of this research.

References and Notes

(1) Foote, C. S. *Science* **1968**, *162*, 963−970.
(2) Renger, G.; Wolff, C. *Biochim. Biophys. Acta* **1977**, *460*, 47−57.
(3) Boucher, F.; van der Rest, M.; Gingras, G. *Biochim. Biophys. Acta* **1977**, *461*, 339−3357.
(4) Foote, C. S.; Chang, Y. C.; Denny, R. W. *J. Am. Chem. Soc.* **1970**, *92*, 5216−5218.
(5) Krinsky, N. I. Function. In *Carotenoids*; Isler, O., Guttman, G., U. Solms, Eds.; Birkhauser Verlag: Basel, 1971; pp 669−716.
(6) Demmig-Adams, B. *Biochim. Biophys. Acta* **1990**, *1020*, 1−24.
(7) Goedheer, J. C. *Biochim. Biophys. Acta* **1959**, *35*, 1−8.
(8) Goedheer, J. C. *Biochim. Biophys. Acta* **1969**, *172*, 252−265.
(9) Cogdell, R. J. *Philos. Trans. R. Soc. London, Ser. B* **1978**, *284*, 569−79.
(10) Govindjee; Govindjee, R. Bioenergetics of photosynthesis. In *Cell Biology*; Govindjee, Ed.; Academic Press: New York, 1975; pp 2−50.
(11) Frank, H. A.; Christensen, R. L. Singlet energy transfer from carotenoids to bacteriochlorophylls. In *Anoxygenic Photosynthetic Bacteria*; Blankenship, R. E., Madigan, M. T., Bauer, C. E., Eds.; Kluwer Academic Publishers: Dordrecht, The Netherlands, 1995; Vol. 2, pp 373−84.
(12) Kirmaier, C.; Holten, D. *Photosynth. Res.* **1987**, *13*, 225−260.
(13) Lang, H. P.; Hunter, C. N. *Biochem. J.* **1994**, *298*, 197−205.
(14) Sandonà, D.; Croce, R.; Pagano, A.; Crimi, M.; Bassi, R. *Biochim. Biophys. Acta* **1998**, *1365*, 207−214.
(15) Yamamoto, H.; Bassi, R. Carotenoids: Localisation and function. In *Oxygenic Photosynthesis: The light reactions*; Ort, D. R., Yocum, C. F., Eds.; Kluwer Academic Publishers: Dordrecht, 1996; pp 539−563.
(16) Snyder, R.; Arvidson, E.; Foote, C.; Harrigan, L.; Christensen, R. L. *J. Am. Chem. Soc.* **1985**, *107*, 4117−4122.
(17) Frank, H. A.; Cua, A.; Chynwat, V.; Young, A.; Gosztola, D.; Wasielewski, M. R. *Photosynth. Res.* **1994**, *41*, 389−395.
(18) Beddard, G. S.; Davidson, R. S.; Tretheway, K. R. *Nature* **1977**, *267*, 373−374.
(19) Gust, D.; Moore, T. A.; Moore, A. L.; Devadoss, C.; Liddell, P. A.; Heman, R.; Nieman, R. A.; Demanche, L. J.; Degraziano, J. M.; Gouni, I. *J. Am. Chem. Soc.* **1992**, *114*, 3591−3603.
(20) Cardoso, S. L.; Nicodem, D. E.; Moore, T. A.; Moore, A. L.; Gust, D. *J. Brazil. Chem. Soc.* **1996**, *7*, 19−30.
(21) Yamamoto, H. Y. *Pure Appl. Chem.* **1979**, *51*, 639−648.
(22) Vrettos, J. S.; Stewart, D. H.; de Paula, J. C.; Brudvig, G. W. *J. Phys. Chem. B* **1999**, *103*, 6403−6406.
(23) Deligiannakis, Y.; Hanley, J.; Rutherford, A. W. *J. Am. Chem. Soc.* **2000**, *122*, 400−401.
(24) Hanley, J.; Deligiannakis, Y.; Pascal, A.; Faller, P.; Rutherford, A. W. *Biochemistry* **1999**, *38*, 8189−8195.
(25) Tracewell, C. A.; Vrettos, J. S.; Bautista, J. A.; Frank, H. A.; Brudvig, G. W. *Arch. Biochem. Biophys.* **2001**, *385*, 61−69.
(26) Sashima, T.; Nagae, H.; Kuki, M.; Koyama, Y. *Chem. Phys. Lett.* **1999**, *299*, 187−194.
(27) Sashima, T.; Koyama, Y.; Yamada, T.; Hashimoto, H. *J. Phys. Chem. B* **2000**, *104*, 5011−5019.
(28) Koyama, Y.; Fujii, R. Cis−trans carotenoids in photosynthesis: Configurations, excited-state properties and physiological functions. In *The Photochemistry of Carotenoids*; Frank, H. A., Young, A. J., Britton, G., Cogdell, R. J., Eds.; Kluwer Academic Publishers: Dordrecht, 1999; Vol. 8, pp 161−188.
(29) Andersson, P. O.; Bachilo, S. M.; Chen, R.-L.; Gillbro, T. *J. Phys. Chem.* **1995**, *99*, 16199−16209.
(30) Andersson, P. O.; Gillbro, T.; Asato, A. E.; Liu, R. S. H. *J. Lumin.* **1992**, *51*, 11−20.
(31) Polivka, T.; Herek, J. L.; Zigmantas, D.; Akerlund, H. E.; Sundstrom, V. *Proc. Natl. Acad. Sci. U.S.A.* **1999**, *96*, 4914−4917.
(32) Polivka, T.; Zigmantas, D.; Frank, H. A.; Bautista, J. A.; Herek, J. L.; Koyama, Y.; Fujii, R.; Sundstrom, V. *J. Phys. Chem. B* **2001**, *105*, 1072−1080.
(33) Sashima, T.; Shiba, M.; Hashimoto, H.; Nagae, H.; Koyama, Y. *Chem. Phys. Lett.* **1998**, *290*, 36−42.
(34) Fujii, R.; Onaka, K.; Kuki, M.; Koyama, Y.; Watanabe, Y. *Chem. Phys. Lett.* **1998**, *288*, 847−853.
(35) Fujii, R.; Onaka, K.; Nagae, H.; Koyama, Y.; Watanabe, Y. *J. Luminescence* **2001**, *92*, 213−222.
(36) Hundle, B. S.; O'Brien, D. A.; Beyer, P.; Kleinig, H.; Hearst, J. E. *FEBS Lett.* **1993**, *315*, 329−334.
(37) Christensen, R. L.; Goyette, M.; Gallagher, L.; Duncan, J.; DeCoster, B.; Lugtenburg, J.; Jansen, F. J.; Hoef, I. v. d. *J. Phys. Chem. A* **1999**, *103*, 2399−2407.
(38) Jansen, F. J. H. M.; Lugtenburg, J. In *Carotenoids*; Britton, G., Liaaen-Jensen, S., Pfander, H., Eds.; Birkhäuser-Verlag: Basel, 1996; Vol. II, pp 233−258.
(39) Fujiwara, K.; Takahashi, H.; Ohta, M. *Bull. Chem. Soc. Jpn.* **1962**, *35*, 1743−1744.
(40) Gebhard, R.; Van der Hoef, K.; Lefeber, A. W. M.; Erkelens, C.; Lugtenburg, J. *Recl. Trav. Chim. Pays-Bas* **1990**, *109*, 378−87.
(41) Gebhard, R.; Van Dijk, J. T. M.; Van Ouwerkerk, E.; Boza, M. V. T. J.; Lugtenburg, J. *Recl. Trav. Chim. Pays-Bas* **1991**, *110*, 459−469.
(42) Gebhard, R.; Van Dijk, J. T. M.; Boza, M. V. T. J.; Van der Hoef, K.; Lugtenburg, J. *Recl. Trav. Chim. Pays-Bas* **1991**, *110*, 332−341.
(43) Benfey, D. B.; Brown, D. C.; Davis, S. J.; Piper, L. G.; Fouter, F. R. *Appl. Opt.* **1992**, *31*, 7034−7040.
(44) Demas, J. N.; Crosby, G. A. *J. Phys. Chem.* **1971**, *75*, 991.
(45) Gosztola, D.; Yamada, H.; Wasielewski, M. R. *J. Am. Chem. Soc.* **1995**, *117*, 2041−2048.
(46) Greenfield, S. R.; Wasielewski, M. R. *Opt. Lett.* **1995**, *20*, 1394−1396.
(47) Lakowicz, J. R. *Principles of Fluorescence Spectroscopy*, 2nd ed.; Kluwer Academic: Plenum Publishers: New York, 1999.
(48) Dale, J. *Acta Chem. Scand.* **1954**, *8*, 1235−1256.
(49) *Cis−trans isomeric carotenoids, vitamin A, and arylpolyenes*; Zechmeister, L., Ed.; Academic Press: New York, 1962.
(50) Cosgrove, S. A.; Guite, M. A.; Burnell, T. B.; Christensen, R. L. *J. Phys. Chem.* **1990**, *94*, 8118−8124.
(51) DeCoster, B.; Christensen, R. L.; Gebhard, R.; Lugtenburg, J.; Farhoosh, R.; Frank, H. A. *Biochim. Biophys. Acta* **1992**, *1102*, 107−114.
(52) Andersson, P. O.; Gillbro, T. *J. Chem. Phys.* **1995**, *103*, 2509−2519.
(53) Englman, R.; Jortner, J. *Mol. Phys.* **1970**, *18*, 145−164.

(54) Turro, N. J. *Modern Molecular Photochemistry*; University Science Books: Mill Valley, CA, 1991.
(55) Frank, H. A.; Desamero, R. Z. B.; Chynwat, V.; Gebhard, R.; van der Hoef, I.; Jansen, F. J.; Lugtenburg, J.; Gosztola, D.; Wasielewski, M. R. *J. Phys. Chem. A* **1997**, *101*, 149−157.
(56) Orlandi, G.; Zerbetto, F.; Zgierski, M. Z. *Chem. Rev.* **1991**, *91*, 867−891.
(57) Tavan, P.; Schulten, K. *J. Chem. Phys.* **1979**, *70*, 5407−5413.
(58) Christensen, R. L. The electronic states of carotenoids. In *The Photochemistry of Carotenoids*; Frank, H. A., Young, A. J., Britton, G., Cogdell, R. J., Eds.; Kluwer Academic Publishers: Dordrecht, 1999; Vol. 8, pp 137−159.
(59) Geldorf, P. A.; Rettschnick, R. P. H.; Hoytink, G. *Chem. Phys. Lett.* **1971**, *10*, 549−558.
(60) Petek, H.; Bell, A. J.; Choi, Y. S.; Yoshihara, K.; Tounge, B. A.; Christensen, R. L. *J. Chem. Phys.* **1995**, *102*, 4726−4739.
(61) Christensen, R. L.; Kohler, B. E. *J. Chem. Phys.* **1976**, *80*, 2197−2200.
(62) Knoll, K.; Schrock, R. R. *J. Am. Chem. Soc.* **1989**, *111*, 7989−8004.
(63) Zechmeister, L.; Polgar, A. *J. Am. Chem. Soc.* **1943**, *65*, 1522−1528.
(64) Zechmeister, L.; LeRosen, A. L.; Schroeder, W. A.; Polgar, A.; Pauling, L. *J. Am. Chem. Soc.* **1943**, *65*, 1940−1951.
(65) Andersson, P. O.; Gillbro, T. *Laser Spectroscopy of Biomolecules* **1992**, *1921*, 48−56.
(66) Chynwat, V.; Frank, H. A. *Chem. Phys.* **1995**, *194*, 237−44.
(67) Wasielewski, M. R.; Kispert, L. D. *Chem. Phys. Lett.* **1986**, *128*, 238−243.
(68) Simpson, J. H.; McLaughlin, L.; Smith, D. S.; Christensen, R. L. *J. Chem. Phys.* **1987**, *87*.
(69) Griesser, H. J.; Wild, U. P. *Chem. Phys.* **1980**, *52*, 117.
(70) Wagner, B. D.; Tittelbach-Helmrich, D.; Steer, R. P. *J. Phys. Chem.* **1992**, *96*, 7904.
(71) Frank, H. A.; Bautista, J. A.; Josue, J. S.; Young, A. J. *Biochemistry* **2000**, *39*, 2831−2837.
(72) Hudson, B.; Kohler, B. *Annu. Rev. Phys. Chem.* **1974**, *25*, 437−460.
(73) Shreve, A. P.; Trautman, J. K.; Frank, H. A.; Owens, T. G.; Albrecht, A. C. *Biochim. Biophys. Acta* **1991**, *1058*, 280−288.
(74) Macpherson, A. N.; Arellano, J. B.; Fraser, N. J.; Cogdell, R. J.; Gillbro, T. *Biophys. J.* **2001**, *80*, 923−930.
(75) Britton, G.; Liaaen-Jensen, S.; Pfander, H. *Carotenoids*; Birkhäuser: Basel, 1995; Vol. 1B.